Supplemental Information for:

The Importance of Morphology on the Activity of Lead Cathodes for the Reduction of Carbon Dioxide to Formate

James E. Pander III, Jeremy Wei Jian Lum, Boon Siang Yeo*

Department of Chemistry, Faculty of Science, National University of Singapore, 3 Science Drive 3, Singapore 117543

*Author to whom correspondence should be addressed to: chmyeos@nus.edu.sg

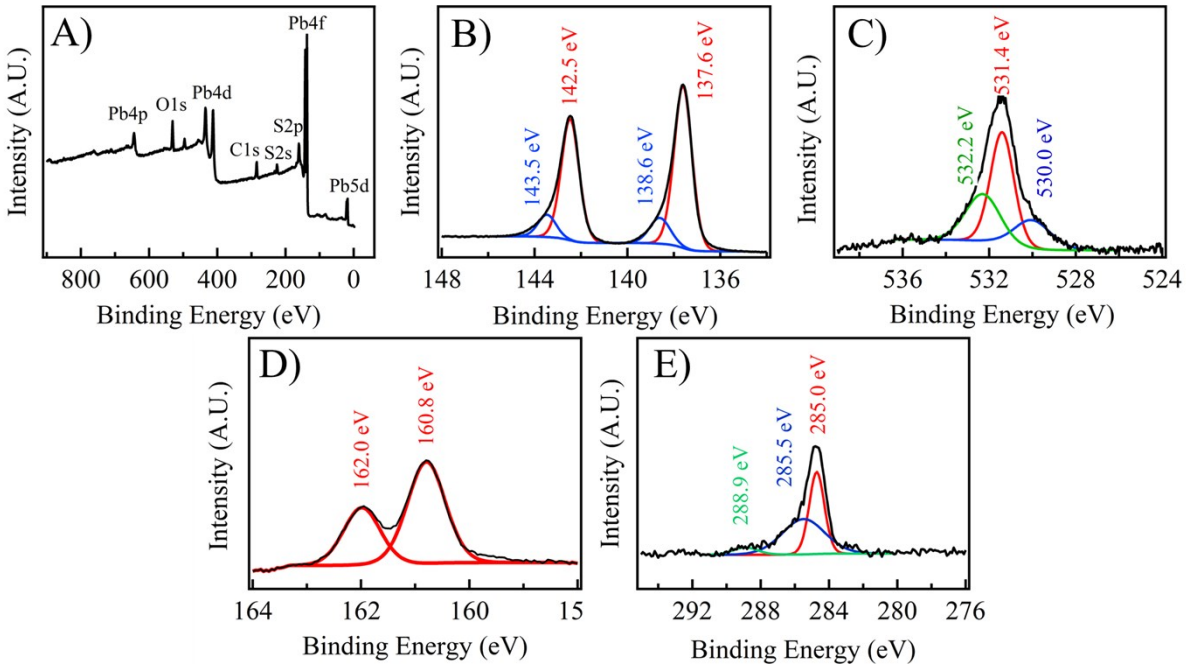

Figure S1: XPS spectra for a freshly prepared PbS sample. (A) Survey scan of all regions; (B) Pb 4f region; (C) O 1s region; (D) S 2p region; (E) C 1s region.

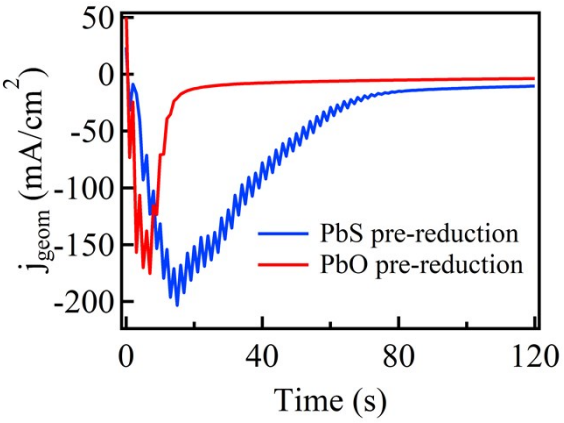

Figure S2: Representative chronoamperograms of PbS sample (blue trace) and PbO (red trace) being reduced to SD-Pb and OD-Pb, respectively, at -0.89 V vs. RHE in 0.1 M $KHCO_3$ without CO_2.

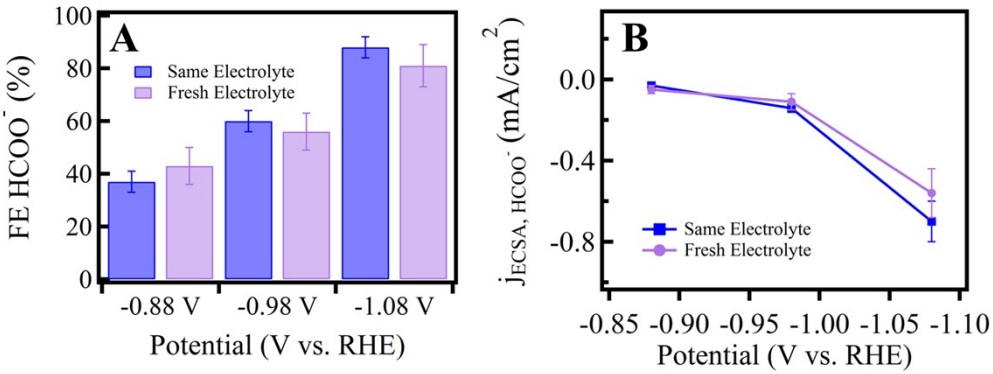

Figure S3: Comparison of (A) Faradaic efficiency for the production of formate and (B) ECSA-normalized current density of formate on SD-Pb electrodes when the same electrolyte was used for both pre-reduction and electrolysis (blue) and when fresh electrolyte solution was used for the electrolysis (purple).

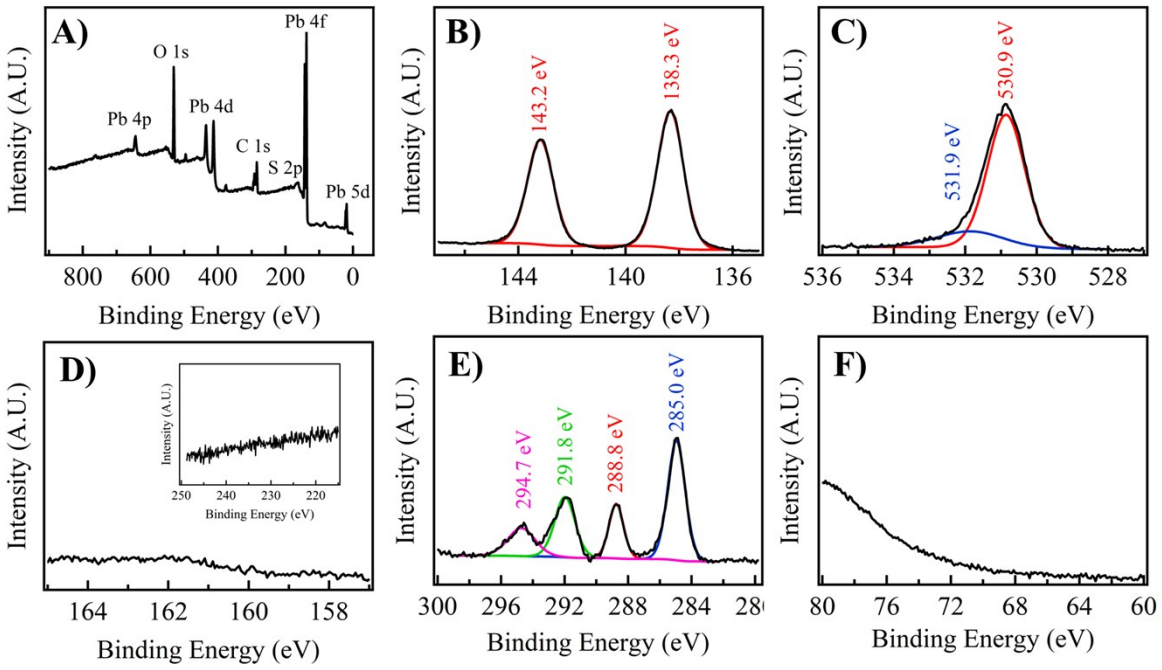

Figure S4: XPS spectra for a SD-Pb sample after pre-reduction. (A) Survey scan of all regions; (B) Pb 4f region; (C) O 1s region; (D) S 2p region (inset shows S 2s region); (E) C 1s region (Peaks at 291.8 eV and 294.7 eV due to residual K^+ adsorbed to the surface during pre-reduction); (F) Pt 4f region.

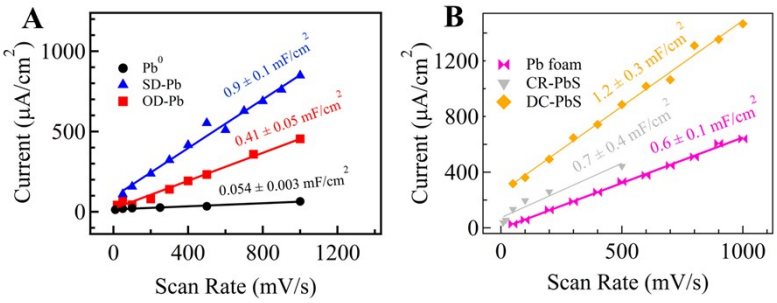

Material	Capacitance (mF/cm²)	Roughness Factor
Polished Pb^0	0.054 ± 0.003	1.00 ± 0.06
OD-Pb	0.41 ± 0.05	8 ± 1
SD-Pb	0.9 ± 0.1	17 ± 2
CR-PbS	0.7 ± 0.4	13 ± 7
DC-PbS	1.2 ± 0.3	22 ± 5
Pb foam	0.6 ± 0.1	12 ± 2

Figure S5: Surface roughness determination for electrodes of interest using double layer capacitance. (A) SD-Pb, OD-Pb, and polished Pb^0; (B) electrodeposited Pb foam, DC-PbS, and CR-PbS. The plots are of representative capacitive current density vs scan rate data for each electrode in 0.1 M $KHCO_3$ at -0.89 V vs. RHE. The table reports capacitance values and roughness factors for each material. Each material is normalized to the capacitance of polished Pb^0.

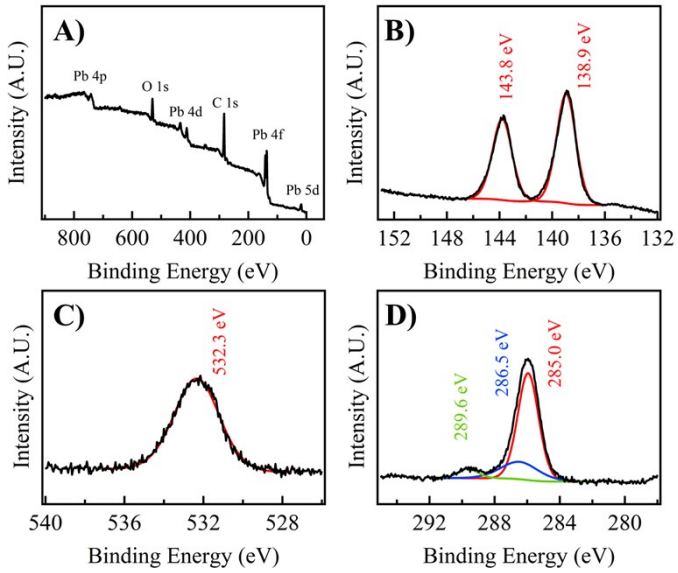

Figure S6: XPS spectra for a polished Pb sample. (A) Survey scan of all regions; (B) Pb 4f region; (C) O 1s region; (D) C 1s region.

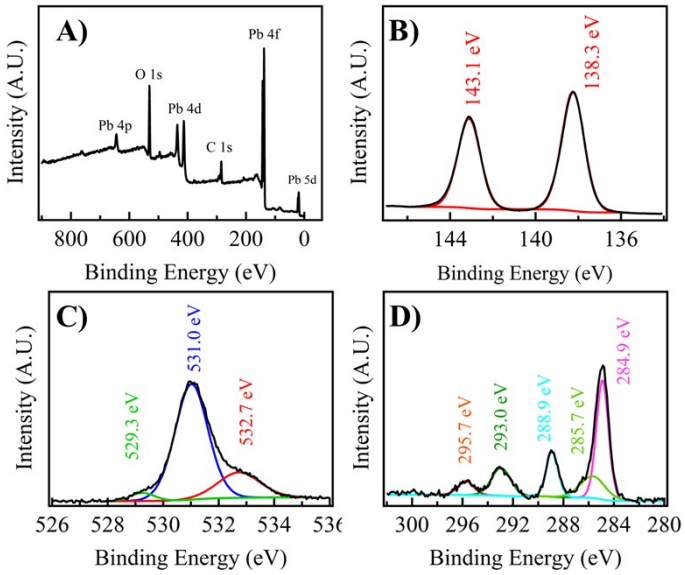

Figure S7: XPS spectra for an OD-Pb sample after pre-reduction. (A) Survey scan of all regions; (B) Pb 4f region; (C) O 1s region; (D) C 1s region (Peaks at 293.0 eV and 295.7 eV due to residual K^+ adsorbed to the surface during pre-reduction).

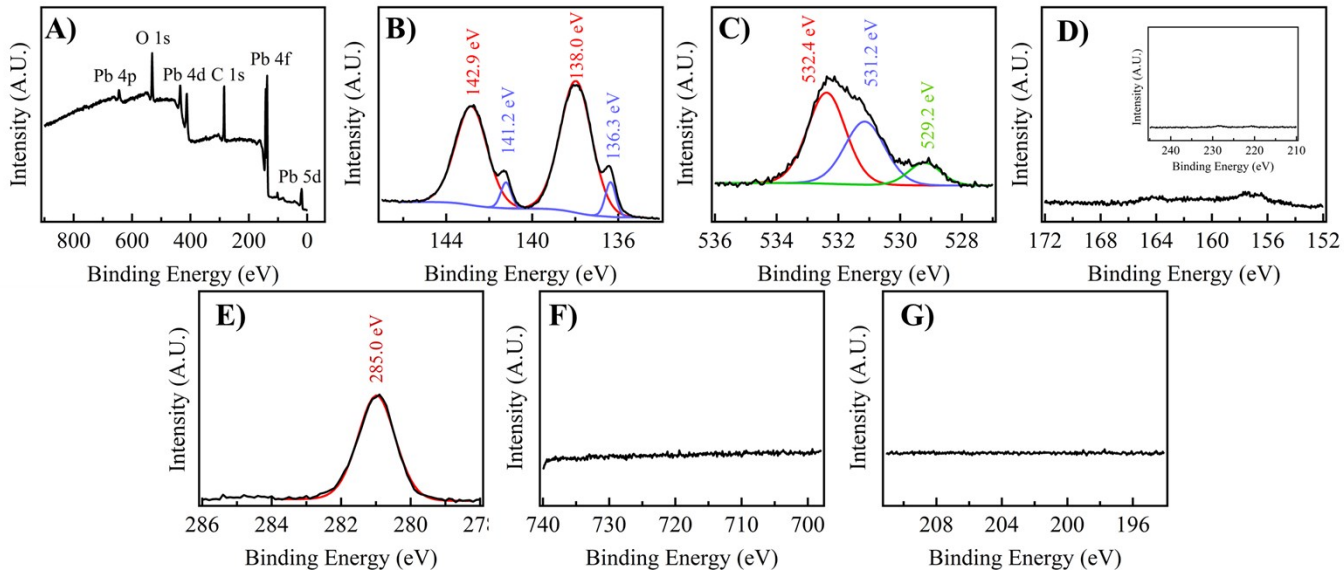

Figure S8: XPS spectra for a CR-PbS sample (after reduction in $FeCl_3$ bath). (A) Survey scan of all regions; (B) Pb 4f region; (C) O 1s region; (D) S 2p region. The small features observable are due to the overlapping Pb 5s region. The inset shows S 2s region to confirm the lack of sulfur signal. (E) C 1s region; (F) Fe 2p region; (G) Cl 2p region.

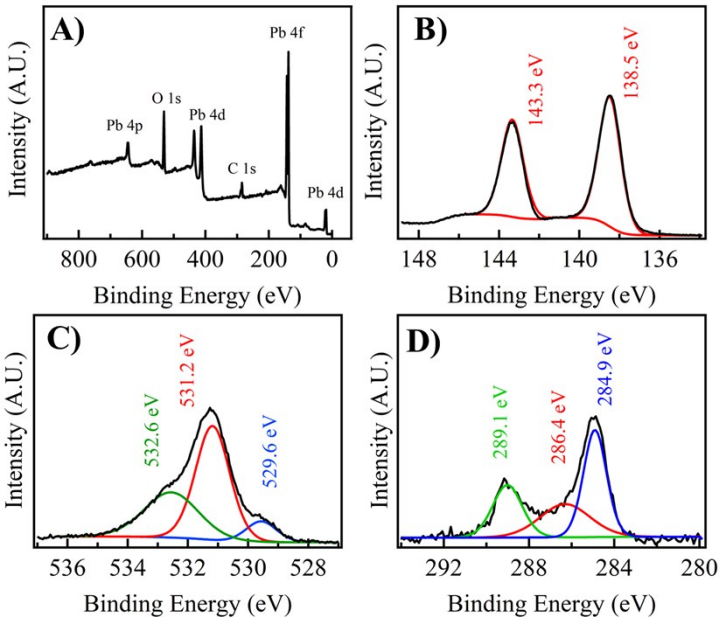

Figure S9: XPS spectra for Pb foam electrodeposited at -0.2 A for 150 s. (A) Survey scan of all regions; (B) Pb 4f region; (C) O 1s region; (D) C1s region.

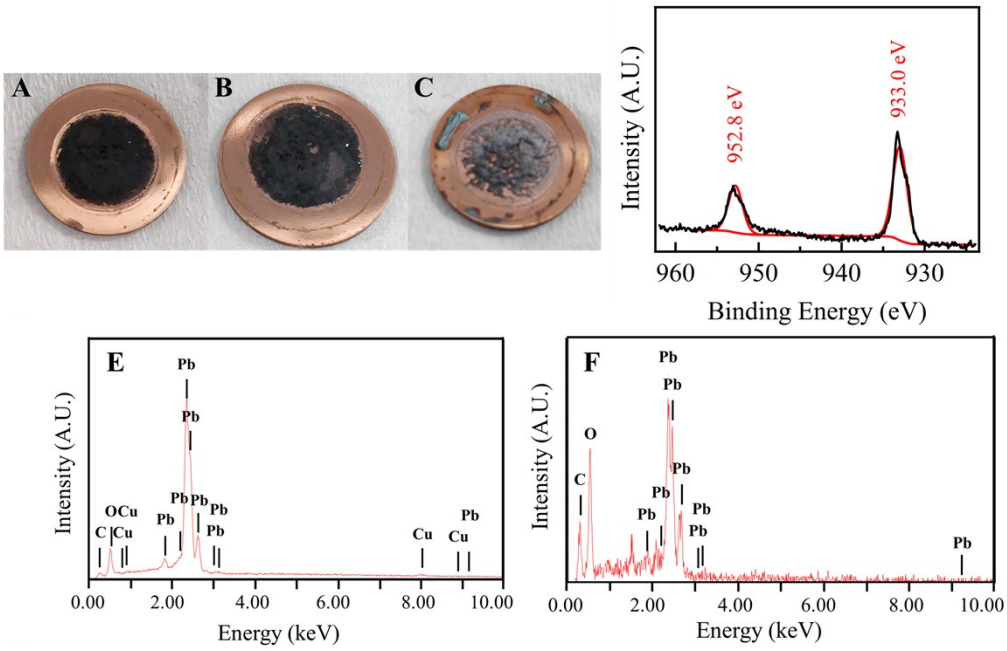

Figure S10: Image of Pb foam (A) freshly prepared, (B) after SEM analysis, and (C) after XPS analysis. (D) XPS of Cu 2p region of Pb foam sample. The large Cu signal in the XPS is likely related to the visibly exposed Cu caused by the ultrahigh vacuum of the XPS chamber, as is evident in image C. (E) EDX analysis of freshly prepared Pb foam sample. Cu was found to be present at <0.3 atom%. (F) EDX analysis of Pb foam that has been removed from the copper substrate. No signal due to the presence of Cu is observed. Based on the EDX results in conjunction with the lack of higher order CO_2RR products, we conclude that Cu is not present in the Pb foam or contributing to the electrochemistry.

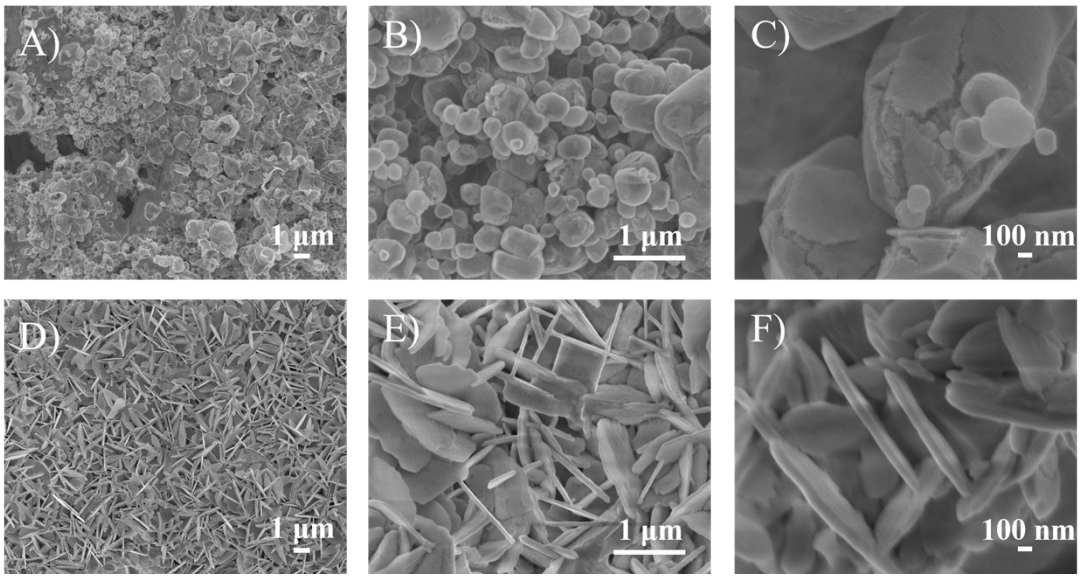

Figure S11: Additional SEM images of PbS precursor (A-C) before pre-reduction at various magnifications; (D-F) SD-Pb (after pre-reduction) at various magnifications.

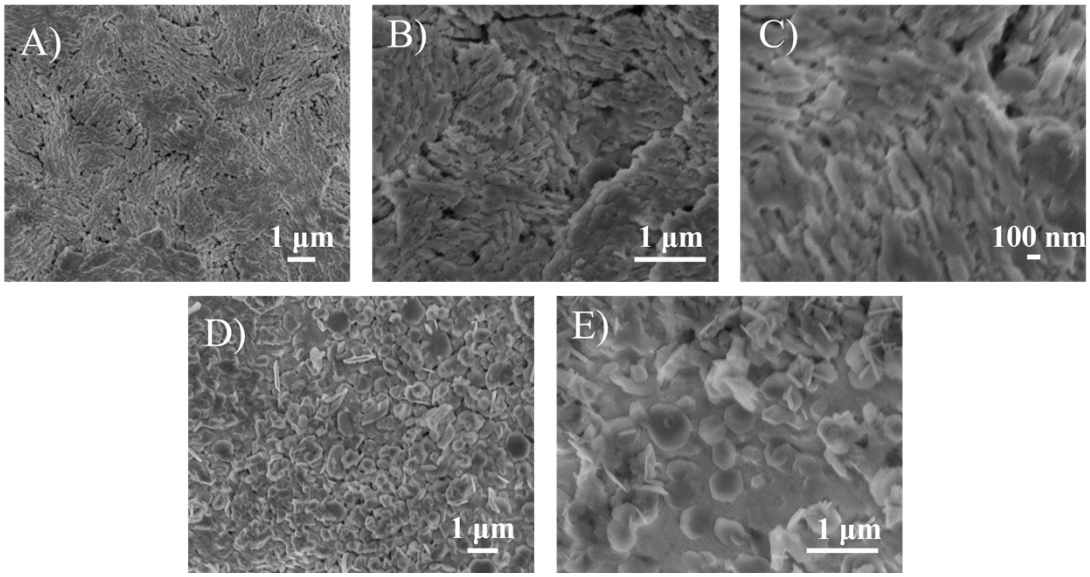

Figure S12: Additional SEM images of (A-C) PbO precursor (before pre-reduction) at various magnifications; (D-E) OD-Pb (after pre-reduction) at various magnifications.

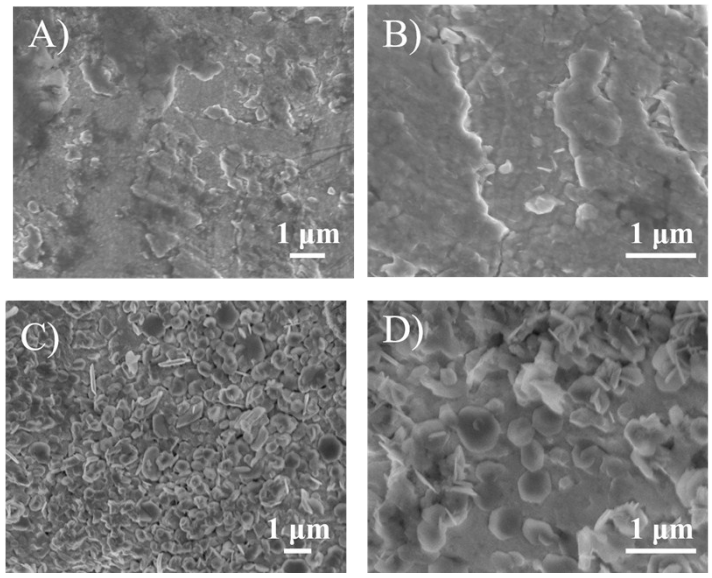

Figure S13: Additional SEM images of (A-B) polished Pb substrate at various magnifications; (C-D) polished Pb substrate after pre-reduction at various magnifications.

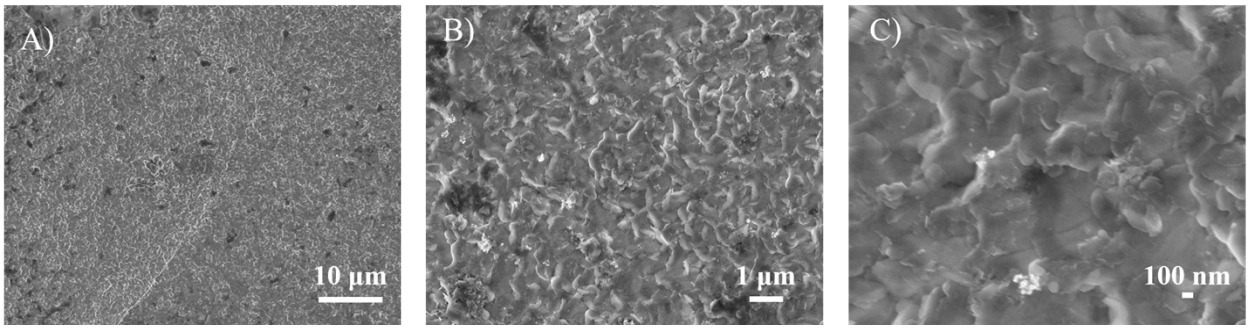

Figure S14: Additional SEM images of (A-C) CR-PbS cathode (after chemical reduction) at various magnifications.

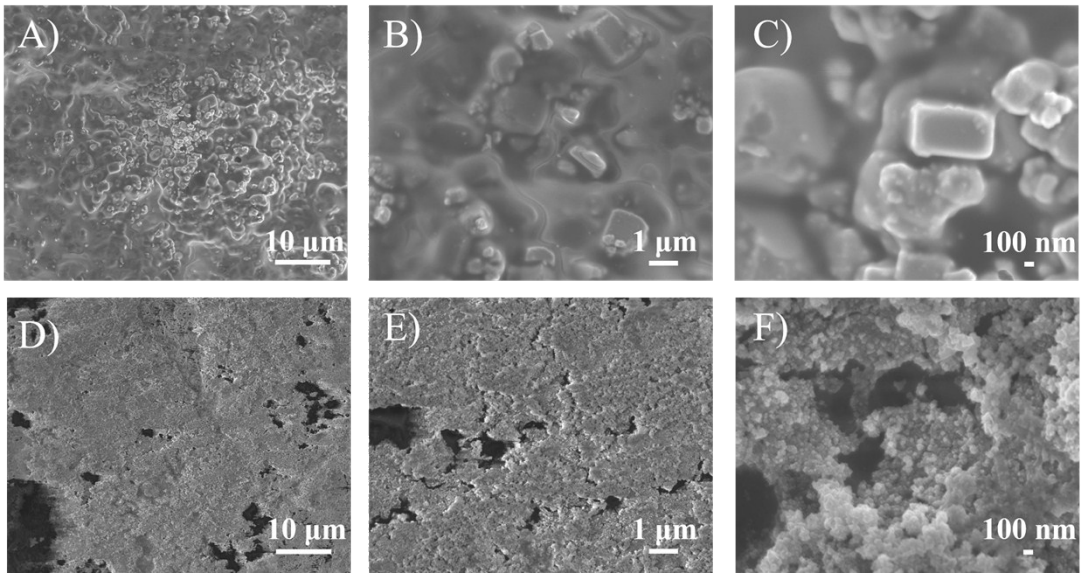

Figure S15: Additional SEM images of (A-C) DC-PbS on a graphite substrate (before pre-reduction) at various magnifications; (D-F) after pre-reduction at various magnifications.

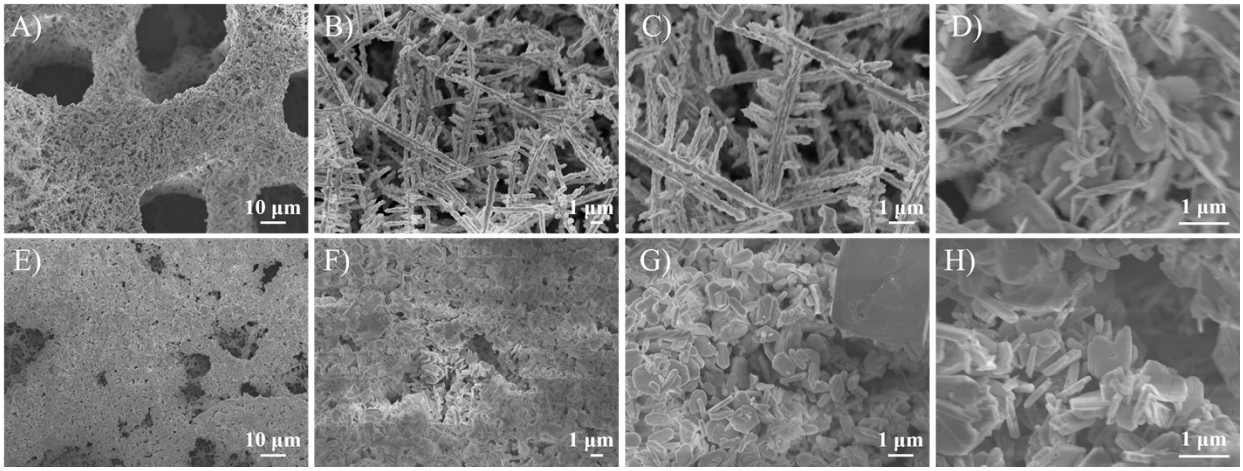

Figure S16: Additional SEM images of Pb foam electrodeposited at -0.2 A for 150 seconds onto a Cu substrate. (A-D) before pre-reduction at various magnifications; (E-H) after pre-reduction at various magnifications.

The current density and Faradaic efficiency data for the SD-Pb, OD-Pb, and Pb cathodes presented in Figure 3 are listed in Tables S1-S3. Total FE values at low overpotential tend to be < 100% due to low current densities causing product detection to occur at the extreme of the calibration curves.

Table S1: Table of currents and Faradaic efficiencies for SD-Pb electrodes (roughness factor 17 ± 2).

Potential (V vs. RHE)	Total Geometric Current Density (mA/cm^2)	ECSA-normalized Total Current Density (mA/cm^2)	Faradaic Efficiency for Formate (%)	Faradaic Efficiency for CO (%)	Faradaic Efficiency for H_2 (%)
-0.83	-0.63 ± 0.05	-0.037 ± 0.005	54 ± 14	0.25 ± 0.02	19 ± 18
-0.88	-1.3 ± 0.3	-0.07 ± 0.02	37 ± 4	0.4 ± 0.2	64 ± 15
-0.93	-2.5 ± 0.4	-0.15 ± 0.03	55 ± 1	0.5 ± 0.1	54 ± 6
-0.98	-4.0 ± 0.6	-0.23 ± 0.04	60 ± 4	0.4 ± 0.2	43 ± 10
-1.03	-8.3 ± 0.2	-0.49 ± 0.06	86 ± 6	0.15 ± 0.08	13 ± 2
-1.08	-13 ± 2	-0.8 ± 0.1	88 ± 4	0.17 ± 0.05	12 ± 7
-1.13	-10 ± 2	-0.6 ± 0.1	89 ± 6	0.08 ± 0.01	8 ± 4
-1.18	-14 ± 3	-0.8 ± 0.2	76 ± 11	0.06 ± 0.02	21 ±12

Table S2: Table of currents and Faradaic efficiencies for OD-Pb electrodes (roughness factor 8 ± 1).

Potential (V vs. RHE)	Total Geometric Current Density (mA/cm^2)	ECSA-normalized Total Current Density (mA/cm^2)	Faradaic Efficiency for Formate (%)	Faradaic Efficiency for CO (%)	Faradaic Efficiency for H_2 (%)
-0.83	-0.35 ± 0.09	-0.04 ± 0.01	27 ± 13	0.36 ± 0.09	9 ± 9
-0.88	-0.5 ± 0.3	-0.07 ± 0.05	46 ± 6	0.5 ± 0.2	29 ± 29
-0.93	-1.0 ± 0.3	-0.13 ± 0.04	55 ± 15	0.9 ± 0.7	22 ± 15
-0.98	-1.5 ± 0.1	-0.18 ± 0.03	72 ± 9	0.5 ± 0.3	17 ± 8
-1.03	-2.1 ± 0.2	-0.26 ± 0.04	53 ± 11	1 ± 1	38 ± 17
-1.08	-3.1 ± 0.2	-0.39 ± 0.06	64 ± 5	0.7 ± 0.3	37 ± 12
-1.13	-5.2 ± 0.7	-0.7 ± 0.1	76 ± 6	0.3 ± 0.2	16 ± 5
-1.18	-11.8 ± 0.4	-1.5 ± 0.2	66 ± 9	0.06 ± 0.06	24 ± 8

Table S3: Table of currents and Faradaic efficiencies for Pb electrodes (roughness factor 1.0 ± 0.06).

Potential (V vs. RHE)	Total Geometric Current Density (mA/cm^2)	ECSA-normalized Total Current Density (mA/cm^2)	Faradaic Efficiency for Formate (%)	Faradaic Efficiency for CO (%)	Faradaic Efficiency for H_2 (%)
-0.83	-0.10 ± 0.05	-0.10 ± 0.05	N.D.	N.D.	N.D.
-0.88	-0.26 ± 0.02	-0.26 ± 0.02	N.D.	N.D.	N.D.
-0.93	-0.37 ± 0.08	-0.37 ± 0.08	18 ± 5	0.30 ± 0.2	38 ± 26
-0.98	-0.76 ± 0.08	-0.76 ± 0.08	16 ± 2	0.3 ± 0.3	61 ± 17
-1.03	-0.9 ± 0.1	-0.9 ± 0.1	32.9 ± 0.2	0.2 ± 0.2	59 ± 15
-1.08	-1.33 ± 0.09	-1.33 ± 0.09	29 ± 1	1 ± 1	58 ± 7
-1.13	-2.5 ± 0.1	-2.5 ± 0.1	41 ± 4	0.5 ± 0.2	33 ± 12
-1.18	-4.3 ± 0.8	-4.3 ± 0.8	64 ± 14	0.3 ± 0.2	29 ± 14

Sample Error Calculation for ECSA-normalized Partial Current Density:

Reported errors are calculated using the standard propagation of error equation:

$$\delta R = |R| \sqrt{\left(\frac{\delta X}{X}\right)^2 + \left(\frac{\delta Y}{Y}\right)^2 + \left(\frac{\delta Z}{Z}\right)^2} \quad \text{(Eqn. S1)}$$

where δ denotes the standard deviation for a measurement (i.e. δX represents the standard deviations for measurement X). For example, the errors on the reported roughness factor of SD-Pb includes the errors from the capacitance measurement for SD-Pb, but also from the samples to which it is normalized:

$$RF_{SD-Pb} = \frac{C_{SD-Pb}}{C_{Pb}} = \frac{0.9\ mF}{0.054\ mF} = 17 \quad \text{(Eqn. S2)}$$

$$\delta RF_{SD-Pb} = |RF_{SD-Pb}| \sqrt{\left(\frac{\delta C_{SD-Pb}}{C_{SD-Pb}}\right)^2 + \left(\frac{\delta C_{Pb}}{C_{Pb}}\right)^2} = 17 \sqrt{\left(\frac{0.1}{0.9}\right)^2 + \left(\frac{0.003}{0.054}\right)^2} = 2 \quad \text{(Eqn. S3)}$$

where RF is the roughness factor and C is the double layer capacitance.

Errors for ECSA-normalized partial current densities were calculated using the cumulative errors from the deviations in the measured total geometric current densities, Faradaic efficiencies, and roughness factors. For example, from Table S2 we have that at -1.03 V vs. RHE, SD-Pb has a geometric total current density of -8.3 ± 0.2 mA, a Faradaic efficiency of 86 ± 6, and a roughness factor of 17 ± 2. Thus, the error calculation is:

$$j_{int} = \frac{j_{geom} * FE}{RF} = \frac{-8.3 * 0.86}{17} = -0.42 \quad \text{(Eqn. S4)}$$

$$\delta j_{int} = |j_{int}| \sqrt{\left(\frac{\delta j_{geom}}{j_{geom}}\right)^2 + \left(\frac{\delta FE}{FE}\right)^2 + \left(\frac{\delta RF}{RF}\right)^2} = |-0.42| \sqrt{\left(\frac{0.2}{-8.3}\right)^2 + \left(\frac{0.06}{0.86}\right)^2 + \left(\frac{2}{17}\right)^2} = 0.06 \quad \text{(Eqn. S5)}$$

Table S4: Selective catalysts for the reduction of CO_2 to $HCOO^-$ (N.R.: data was not reported).

Electrode	Electrolyte	Applied Potential (V vs. RHE)	Total j_{geom} (mA/cm^2)	FE_{HCOO^-} (%)	FE_{CO} (%)	Reference
SD-Pb	0.1 M $KHCO_3$	-1.08	-13	88	0.17	This work
Pb	0.1 M $KHCO_3$	-1.08	-1.33	29	1	This work
OD-Pb	0.1 M $KHCO_3$	-1.08	-3.1	64	0.7	This work
Pb	0.1 M K_2CO_3	-1.1	-0.5	40	N.R.	1
Pb	0.5 M NaOH	-0.95	-2.5	70	N.R.	2
OD-Pb	0.5 M $KHCO_3$	-1.0	-4	100	N.R.	3
Sn/SnO_x	0.5 M $KHCO_3$	-0.7	N.R.	60	40	4
Sn Porous Nanowires	0.1 M $KHCO_3$	-1.0	-6	80	10	5
Sn GDE	0.1 M $KHCO_3$	-0.6	-3	64	N.R.	6
SnO_2 NP on C black	0.1 M $NaHCO_3$	-1.08	-5.8	85	N.R.	7
SnS_2-derived Sn/rGO	0.5 M KHCO3	-1.05	-13.9	85	5	8
Anodized In	0.5 M K_2SO_4	-1.03	N.R.	80	N.R.	9
In/C GDE	0.1 M K_2SO_4	-1.2	N.R.	35	N.R.	10
S-Doped OD-Cu	0.1 M $KHCO_3$	-0.8	-14.5	74	0	11
Pd NP	0.5 M $KHCO_3$	-0.2	-22	97	N.R.	12

References

(1) F. Köleli, T. Atilan, N. Palamut, A. M. Gizir, R. Aydin, and C. H. J. Hamann, *Appl. Electrochem.* 2003, **33**, 447–450.
(2) B. Innocent, D. Liaigre, D. Pasquier, F. Ropital, J.-M. Léger, and K. B. Kokoh, *J. Appl. Electrochem.*, 2008, **39**, 227–232.
(3) C. H. Lee and M. W. Kanan, *ACS Catal.*, 2015, **5**, 465–469.
(4) Y. Chen and M. W. Kanan, *J. Am. Chem. Soc.*, 2012, **134**, 1986–1989.
(5) B. Kumar, V. Atla, J. P. Brian, S. Kumari, T. Q. Nguyen, M. Sunkara, and J. M. Spurgeon, *Angew. Chem. Int. Ed.*, 2017, **56**, 3645–3649.
(6) J. Wu, F. G. Risalvato, P. P. Sharma, P. J. Pellechia, F.-S. Ke, and X.-D. Zhou, *J. Electrochem. Soc.*, 2013, **160**, F953–F957.
(7) R. Zhang, W. Lv, and L. Lei, *Appl. Surf. Sci.*, 2015, **356**, 24–29.
(8) F. Li, L. Chen, M. Xue, T. Williams, Y. Zhang, D. R. MacFarlane, and J. Zhang, *Nano Energy*, 2017, **31**, 270–277.
(9) Z. M. Detweiler, J. L. White, S. L. Bernasek, and A. B. Bocarsly, *Langmuir*, 2014, **30**, 7593–7600.
(10) Z. Bitar, A. Fecant, E. Trela-Baudot, S. Chardon-Noblat, and D. Pasquier, *Appl. Catal. B Environ.*, 2016, **189**, 172–180.
(11) Y. Huang, Y. Deng, A. D. Handoko, G. K. L. Goh, and B. S. Yeo, *ChemSusChem*, 2017, **10**, 1–8.
(12) A. Klinkova, P. De Luna, C.-T. Dinh, O. Voznyy, E. M. Larin, E. Kumacheva, and E. H. Sargent, *ACS Catal.*, 2016, **6**, 8115–8120.